We are IntechOpen, the world's leading publisher of Open Access books Built by scientists, for scientists

4,800
Open access books available

122,000
International authors and editors

135M
Downloads

Our authors are among the

154
Countries delivered to

TOP 1%
most cited scientists

12.2%
Contributors from top 500 universities

CLARIVATE ANALYTICS BOOK CITATION INDEX INDEXED

WEB OF SCIENCE™

Selection of our books indexed in the Book Citation Index in Web of Science™ Core Collection (BKCI)

Interested in publishing with us?
Contact book.department@intechopen.com

Numbers displayed above are based on latest data collected.
For more information visit www.intechopen.com

23

Resolved Acceleration Control for Underwater Vehicle-Manipulator Systems: Continuous and Discrete Time Approach

Shinichi Sagara
Kyushu Institute of Technology
Japan

1. Introduction

Underwater robots, especially Underwater Vehicle-Manipulator Systems (UVMS), are expected to have important roles in ocean exploration (Yuh, 1995). Many studies about dynamics and control of UVMS have been reported (Maheshi et al., 1991; McMillan et al., 1995; McLain et al., 1996; Tarn et al., 1996; Antonelli & Chiaverini, 1998; McLain et al., 1998; Antonelli et al., 2000; Sarkar & Podder, 2001). However, there are only a few experimental studies. Most of the control methods of UVMS have been proposed based on the methods of Autonomous Underwater Vehicles. In these control methods, the desired accelerations and velocities of the end-tip of the manipulator are transformed to the desired manipulator's joint accelerations and velocities only use of the kinematic relation, and the computed torque method with joint angle and angular velocity feedbacks are utilized. In other words, the control methods use errors consisting of task-space signals of vehicle and joint-space signals of manipulator. Therefore, the control performance of the end-effector depends on the vehicle's control performance.

We have proposed continuous-time and discrete-time Resolved Acceleration Control (RAC) methods for UVMS (Yamada & Sagara, 2002; Sagara, 2003; Sagara et al., 2004; Sagara et al., 2006; Yatoh & Sagara, 2007; Yatoh & Sagara, 2008). In our proposed methods, the desired joint values are obtained by kinematic and momentum equations with feedback of task-space signals. From the viewpoint of underwater robot control, parameters and coefficients of hydrodynamic models are generally used as constant values that depend on the shape of the robots (Fossen, 1994). Our proposed methods described above can reduce the influence of the modelling errors of hydrodynamics by position and velocity feedbacks. The effectiveness of the RAC methods has been demonstrated by using a floating underwater robot with vertical planar 2-link manipulator shown in Figure 1.

In this chapter, our proposed continuous-time and discrete-time RAC methods are described and the both experimental results using a 2-link underwater robot are shown. First, we explain about a continuous-time RAC method and show that the RAC method has good control performance in comparison with a computed torque method. Next, to obtain higher control performance, we introduce a continuous-time RAC method with disturbance compensation. In practical systems digital computers are utilized for controllers, but there is no discrete-time control method for UVMS except our proposed methods. Then, we address

Source: Underwater Vehicles, Book edited by: Alexander V. Inzartsev,
ISBN 978-953-7619-49-7, pp. 582, December 2008, I-Tech, Vienna, Austria

discrete time RAC methods including the ways of disturbance compensation and avoiding singular configuration.

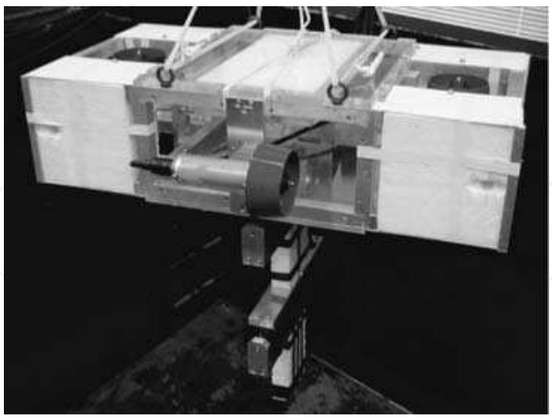

Fig. 1. Vertical type 2-link underwater robot

2. Modelling

The UVMS model used in this chapter is shown in Figure 2. It has a robot base (vehicle) and an *n*-DOF manipulator.

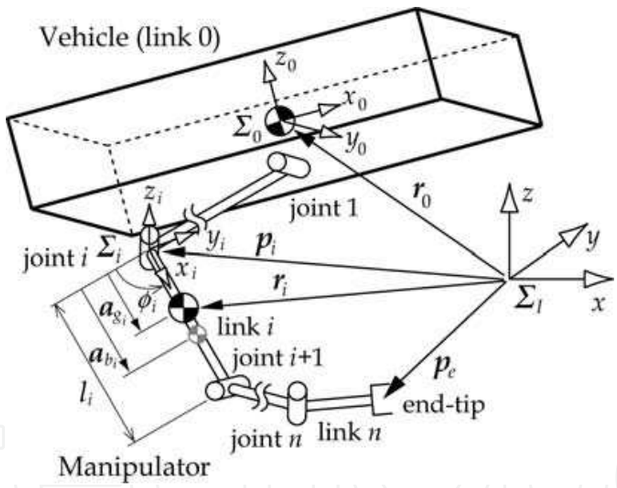

Fig. 2. Model of underwater robot with n-link manipulator

The symbols used in this chapter are defined as follows:

n : number of joints

Σ_I : inertial coordinate frame

Σ_i : link i coordinate frame (i = 0, 1, 2, $\cdots$, n; link 0 means the vehicle)

${}^I\boldsymbol{R}_i$: coordinate transformation matrix from Σ_i to Σ_I

$\boldsymbol{p}_e$: position vector of the end-tip of the manipulator with respect to Σ_I

$\boldsymbol{p}_i$: position vector of the origin of Σ_i with respect to Σ_I

$\boldsymbol{r}_i$: position vector of the center of gravity of link i with respect to Σ_I

ϕ_i : relative angle of joint i

$\boldsymbol{\psi}_0$: roll-pitch-yaw attitude vector of Σ_0 with respect to Σ_I

$\boldsymbol{\psi}_e$: roll-pitch-yaw attitude vector of the end-tip of the manipulator with respect to Σ_I

$\boldsymbol{\omega}_0$: angular velocity vector of Σ_0 with respect to Σ_I

$\boldsymbol{\omega}_e$: angular velocity vector of the end-tip of the manipulator with respect to Σ_I

$\boldsymbol{\phi}$: relative joint angle vector ($=[\phi_1 \quad \cdots \quad \phi_n]^T$)

${}^i\boldsymbol{k}_i$: unit vector indicating a rotational axis of joint i ($=[0 \quad 0 \quad 1]^T$)

m_i: mass of link i

${}^i\boldsymbol{M}_{a_i}$: added mass matrix of link i with respect to Σ_i

${}^i\boldsymbol{I}_i$: inertia tensor of link i with respect to Σ_i

${}^i\boldsymbol{I}_{a_i}$: added inertia tensor of link i with respect to Σ_i

$\boldsymbol{x}_0$: position and orientation vector of Σ_0 with respect to Σ_I ($=[\boldsymbol{r}_0^T \quad \boldsymbol{\Psi}_0^T]^T$)

$\boldsymbol{x}_e$: position and orientation vector of the end-tip with respect to Σ_I ($=[\boldsymbol{p}_e^T \quad \boldsymbol{\Psi}_e^T]^T$)

$\boldsymbol{\nu}_0$: linear and angular vector of Σ_0 with respect to Σ_I ($=[\dot{\boldsymbol{r}}_0^T \quad \boldsymbol{\omega}_0^T]^T$)

$\boldsymbol{\nu}_e$: linear and angular vector of the end-tip with respect to Σ_I ($=[\dot{\boldsymbol{p}}_e^T \quad \boldsymbol{\omega}_e^T]^T$)

l_i: length of link i

$\boldsymbol{a}_{g_i}$: position vector from joint i to the center of gravity of link i with respect to Σ_I

$\boldsymbol{a}_{b_i}$: position vector from joint i to the buoyancy center of link i with respect to Σ_I

D_i : width of link i

V_i : volume of link i

ρ : fluid density

C_{D_i} : drag coefficient of link i

$\boldsymbol{g}$: gravitational acceleration vector

$\boldsymbol{E}_j$: $j \times j$ unit matrix

$\tilde{\ }$: tilde operator stands for a cross product such that $\tilde{\boldsymbol{r}}\boldsymbol{a} = \boldsymbol{r} \times \boldsymbol{a}$

2.1 Kinematics

First, from Figure 2 a time derivative of the end-tip position vector $\dot{\boldsymbol{p}}_e$ is

$$\dot{\boldsymbol{p}}_e = \dot{\boldsymbol{r}}_0 + \tilde{\boldsymbol{\omega}}_0(\boldsymbol{p}_e - \boldsymbol{r}_0) + \sum_{i=1}^{n} \left\{ \tilde{\boldsymbol{k}}_i(\boldsymbol{p}_e - \boldsymbol{p}_i) \right\} \dot{\phi}_i \tag{1}$$

where $\boldsymbol{k}_i = {}^I\boldsymbol{R}_i \, {}^i\boldsymbol{k}_i$.

On the other hand, relationship between end-tip angular velocity and joint velocity is expressed with

$$\boldsymbol{\omega}_e = \boldsymbol{\omega}_0 + \sum_{i=1}^{n} \boldsymbol{k}_i \dot{\phi}_i \ . \tag{2}$$

From Equations (1) and (2) the following equation is obtained:

$$\boldsymbol{\nu}_e = \boldsymbol{A}\boldsymbol{\nu}_0 + \boldsymbol{B}\dot{\boldsymbol{\phi}} \tag{3}$$

where

$$\boldsymbol{A} = \begin{bmatrix} \boldsymbol{E}_3 & -(\tilde{\boldsymbol{p}}_e - \tilde{\boldsymbol{r}}_0) \\ \boldsymbol{0} & \boldsymbol{E}_3 \end{bmatrix},$$

$$\boldsymbol{B} = \begin{bmatrix} \tilde{\boldsymbol{k}}_1(\boldsymbol{p}_e - \boldsymbol{p}_1) & \tilde{\boldsymbol{k}}_2(\boldsymbol{p}_e - \boldsymbol{p}_2) & \cdots & \tilde{\boldsymbol{k}}_n(\boldsymbol{p}_e - \boldsymbol{p}_n) \\ \boldsymbol{k}_1 & \boldsymbol{k}_2 & \cdots & \boldsymbol{k}_n \end{bmatrix}.$$

Next, let $\boldsymbol{\eta}$ and $\boldsymbol{\mu}$ be a linear and an angular momentum of the robot including hydrodynamic added mass tensor ${}^{i}\boldsymbol{M}_{a_i}$ and added inertia tensor ${}^{i}\boldsymbol{I}_{a_i}$ of link *i*. Then

$$\boldsymbol{\eta} = \sum_{i=0}^{n} \boldsymbol{M}_{T_i}\dot{\boldsymbol{r}}_i \,, \tag{4}$$

$$\boldsymbol{\mu} = \sum_{i=0}^{n} \left(\boldsymbol{I}_{T_i}\boldsymbol{\omega}_i + \tilde{\boldsymbol{r}}_i\boldsymbol{M}_{T_i}\dot{\boldsymbol{r}}_i \right) - \boldsymbol{r}_0 \times \boldsymbol{\eta} \tag{5}$$

where $\boldsymbol{M}_{T_i} = m_i\boldsymbol{E}_3 + {}^{I}\boldsymbol{R}_i \, {}^{i}\boldsymbol{M}_{a_i} \, {}^{i}\boldsymbol{R}_I$ and $\boldsymbol{I}_{T_i} = {}^{I}\boldsymbol{R}_i \, ({}^{i}\boldsymbol{I}_i + {}^{i}\boldsymbol{I}_{a_i}) \, {}^{i}\boldsymbol{R}_I$. Here, linear and angular velocities of the center of gravity of link *i* are described as

$$\dot{\boldsymbol{r}}_i = \dot{\boldsymbol{r}}_0 + \tilde{\boldsymbol{\omega}}_0(\boldsymbol{r}_i - \boldsymbol{r}_0) + \sum_{j=1}^{i} \left\{ \tilde{\boldsymbol{k}}_j \left(\boldsymbol{r}_i - \boldsymbol{p}_j \right) \right\} \dot{\phi}_j \,, \tag{6}$$

$$\boldsymbol{\omega}_i = \boldsymbol{\omega}_0 + \sum_{j=1}^{i} \boldsymbol{k}_j \dot{\phi}_j \,. \tag{7}$$

Therefore, the following equation is obtained from Equations (4)-(7):

$$\boldsymbol{s} = \begin{bmatrix} \boldsymbol{\eta} \\ \boldsymbol{\mu} \end{bmatrix} = \boldsymbol{C}\boldsymbol{\nu}_0 + \boldsymbol{D}\dot{\boldsymbol{\phi}} \tag{8}$$

where

$$\boldsymbol{C} = \begin{bmatrix} \sum_{i=0}^{n} \boldsymbol{M}_{T_i} & -\sum_{i=0}^{n} \boldsymbol{M}_{T_i}(\tilde{\boldsymbol{r}}_i - \tilde{\boldsymbol{r}}_0) \\ \sum_{i=0}^{n} (\tilde{\boldsymbol{r}}_i - \tilde{\boldsymbol{r}}_0)\boldsymbol{M}_{T_i} & \sum_{i=0}^{n} \left\{ \boldsymbol{I}_{T_i} - (\tilde{\boldsymbol{r}}_i - \tilde{\boldsymbol{r}}_0)\boldsymbol{M}_{T_i}(\tilde{\boldsymbol{r}}_i - \tilde{\boldsymbol{r}}_0) \right\} \end{bmatrix},$$

$$\boldsymbol{D} = \begin{bmatrix} \boldsymbol{d}_{11} & \boldsymbol{d}_{12} & \cdots & \boldsymbol{d}_{1n} \\ \boldsymbol{d}_{21} & \boldsymbol{d}_{22} & \cdots & \boldsymbol{d}_{2n} \end{bmatrix},$$

$$\boldsymbol{d}_{1i} = \sum_{j=i}^{n} \boldsymbol{M}_{T_j} \tilde{\boldsymbol{k}}_i \left(\boldsymbol{r}_j - \boldsymbol{p}_i \right),$$

$$\boldsymbol{d}_{2i} = \sum_{j=i}^{n} \left\{ \boldsymbol{I}_{T_j} \boldsymbol{k}_i + \left(\tilde{\boldsymbol{r}}_j - \tilde{\boldsymbol{r}}_0 \right) \boldsymbol{M}_{Tj} \tilde{\boldsymbol{k}}_i \left(\boldsymbol{r}_j - \boldsymbol{p}_i \right) \right\}.$$

Here, we assume that the added mass and added inertia are constant. In reality, the added mass and inertia are variable, but the influence of the variation is compensated by a control method given in the following section.

2.2 Equation of motion

First, the drag force and the moment of joint i can generally by represented as follows (Levesque & Richard, 1994):

$$\boldsymbol{f}_{d_i} = \frac{\rho}{2} C_{D_i} D_i {}^{I}\boldsymbol{R}_i \int_0^{l_i} \| \boldsymbol{w}_i \| \boldsymbol{w}_i dx_i \,, \tag{9}$$

$$\boldsymbol{t}_{d_i} = \frac{\rho}{2} C_{D_i} D_i {}^{I}\boldsymbol{R}_i \int_0^{l_i} \hat{\boldsymbol{x}}_i \times \| \boldsymbol{w}_i \| \boldsymbol{w}_i dx_i \tag{10}$$

where

$$\boldsymbol{w}_i = \begin{bmatrix} 0 & \boldsymbol{0} \\ \boldsymbol{0} & \boldsymbol{E}_2 \end{bmatrix} {}^{i}\boldsymbol{R}_I \left(\dot{\boldsymbol{r}}_i + \tilde{\boldsymbol{\omega}}_i \hat{\boldsymbol{x}}_i \right)$$

and $\hat{\boldsymbol{x}}_i = \begin{bmatrix} x_i & 0 & 0 \end{bmatrix}^T$.

Next, the gravitational and buoyant forces acting on link i are described as

$$\boldsymbol{f}_{g_i} = (\rho V_i - m_i)\boldsymbol{g} \,, \tag{11}$$

$$\boldsymbol{t}_{g_i} = (\rho V_i \tilde{\boldsymbol{a}}_{b_i} - m_i \tilde{\boldsymbol{a}}_{g_i})\boldsymbol{g} \,. \tag{12}$$

Considering the hydrodynamic forces described above and using the Newton-Euler formulation, the following equation of motion can be obtained (Antonelli, 2003):

$$\boldsymbol{M}(\boldsymbol{q})\dot{\boldsymbol{\zeta}} + \boldsymbol{N}(\boldsymbol{q}, \boldsymbol{\zeta})\boldsymbol{\zeta} + \boldsymbol{f} = \boldsymbol{u} \tag{13}$$

where

$$\boldsymbol{q} = \begin{bmatrix} \boldsymbol{x}_0 \\ \boldsymbol{\phi} \end{bmatrix}, \ \boldsymbol{\zeta} = \begin{bmatrix} \boldsymbol{v}_0 \\ \dot{\boldsymbol{\phi}} \end{bmatrix}, \ \boldsymbol{u} = \begin{bmatrix} \boldsymbol{f}_{\mathrm{B}} \\ \boldsymbol{\tau}_{\mathrm{B}} \\ \boldsymbol{\tau}_{\mathrm{M}} \end{bmatrix},$$

and $\boldsymbol{M}$ is the inertia matrix including the added mass ${}^{i}\boldsymbol{M}_{a_i}$ and inertia ${}^{i}\boldsymbol{I}_{a_i}$, $\boldsymbol{N}\boldsymbol{\zeta}$ is the vector of the Coliolis and centrifugal forces, $\boldsymbol{f}$ is the vector consisting of the drag and gravitational and buoyant forces and moments, $\boldsymbol{f}_{\mathrm{B}}$ and $\boldsymbol{\tau}_{\mathrm{B}}$ are the force and torque vectors of the vehicle, respectively, and $\boldsymbol{\tau}_{\mathrm{M}}$ is the joint torque vector of manipulator. Moreover, the relationship between $\boldsymbol{\omega}_*$ and $\boldsymbol{\psi}_* = [\psi_{r_*} \quad \psi_{p_*} \quad \psi_{y_*}]^T$ $(* = 0, e)$ is described as

$$\boldsymbol{\omega}_* = \boldsymbol{S}_{\psi_*}\dot{\boldsymbol{\psi}}_* \tag{14}$$

where

$$\boldsymbol{S}_{\psi_*} = \begin{bmatrix} \cos\psi_{p_*}\cos\psi_{y_*} & -\sin\psi_{y_*} & 0 \\ \cos\psi_{p_*}\sin\psi_{y_*} & \cos\psi_{y_*} & 0 \\ \sin\psi_{p_*} & 0 & 1 \end{bmatrix}.$$

Thus, the relationship between $\dot{\boldsymbol{q}}$ and $\boldsymbol{\zeta}$ is described as

$$\boldsymbol{\zeta} = \begin{bmatrix} \boldsymbol{E}_3 & \boldsymbol{0} \\ & \boldsymbol{S}_{\psi_0} \\ \boldsymbol{0} & \boldsymbol{E}_n \end{bmatrix}\dot{\boldsymbol{q}}\,. \tag{15}$$

3. Continuous-time RAC

3.1 RAC law

Differentiating Equations (3) and (8) with respect to time, the following equation can be obtained:

$$\boldsymbol{W}(t)\boldsymbol{\alpha}(t) = \boldsymbol{\beta}(t) + \boldsymbol{\gamma}(t) - \dot{\boldsymbol{W}}(t)\boldsymbol{\zeta}(t) \tag{16}$$

where

$$\boldsymbol{W} = \begin{bmatrix} \boldsymbol{C}+\boldsymbol{E}_6 & \boldsymbol{D} \\ \boldsymbol{A} & \boldsymbol{B} \end{bmatrix},\ \boldsymbol{\alpha} = \dot{\boldsymbol{\zeta}},\ \boldsymbol{\beta} = \begin{bmatrix} \dot{\boldsymbol{\nu}}_0 \\ \dot{\boldsymbol{\nu}}_e \end{bmatrix},\ \boldsymbol{\gamma} = \begin{bmatrix} \dot{\boldsymbol{s}} \\ \boldsymbol{0} \end{bmatrix},$$

and $\dot{\boldsymbol{s}}$ is the external force, including the hydrodynamic force and the thrust of the thruster, which acts on the vehicle.

For Equation (16), the reference acceleration is defined as

$$\boldsymbol{\alpha}^{\mathrm{ref}}(t) = \begin{bmatrix} \dot{\boldsymbol{\nu}}_0^{\mathrm{ref}} \\ \ddot{\boldsymbol{\phi}}^{\mathrm{ref}} \end{bmatrix} = \boldsymbol{W}^{\#}(t)\{\boldsymbol{\beta}^{\mathrm{ref}}(t) + \boldsymbol{\gamma}(t) - \dot{\boldsymbol{W}}(t)\boldsymbol{\zeta}(t)\} \tag{17}$$

where

$$\boldsymbol{\beta}^{\mathrm{ref}} = \begin{bmatrix} \ddot{\boldsymbol{r}}_0^{\mathrm{des}} \\ \dot{\boldsymbol{\omega}}_0^{\mathrm{des}} \\ \ddot{\boldsymbol{p}}_e^{\mathrm{des}} \\ \dot{\boldsymbol{\omega}}_e^{\mathrm{des}} \end{bmatrix} + \boldsymbol{K}_V \begin{bmatrix} \dot{\boldsymbol{r}}_0^{\mathrm{des}} - \dot{\boldsymbol{r}}_0 \\ \boldsymbol{\omega}_0^{\mathrm{des}} - \boldsymbol{\omega}_0 \\ \dot{\boldsymbol{p}}_e^{\mathrm{des}} - \dot{\boldsymbol{p}}_e \\ \boldsymbol{\omega}_e^{\mathrm{des}} - \boldsymbol{\omega}_e \end{bmatrix} + \boldsymbol{K}_P \begin{bmatrix} \boldsymbol{r}_0^{\mathrm{des}} - \boldsymbol{r}_0 \\ \boldsymbol{e}_{\omega_0} \\ \boldsymbol{p}_e^{\mathrm{des}} - \boldsymbol{p}_e \\ \boldsymbol{e}_{\omega_e} \end{bmatrix}, \tag{18}$$

and $\boldsymbol{W}^{\#}$ is the pseudoinverse of $\boldsymbol{W}$, i.e. $\boldsymbol{W}^{\#} = \boldsymbol{W}^T\left(\boldsymbol{W}\boldsymbol{W}^T\right)^{-1}$, and $*^{\mathrm{des}}$ ($* = \boldsymbol{r}_0, \boldsymbol{p}_e, \boldsymbol{\omega}_0, \boldsymbol{\omega}_e$) is the desired value of $*$, $\boldsymbol{K}_V$ and $\boldsymbol{K}_P$ are diagonal matrices consisting of scalar gain constants. Moreover,

$$\boldsymbol{e}_{\omega_*} = \frac{1}{2}\left(\boldsymbol{i}_* \times \boldsymbol{i}_{*_d} + \boldsymbol{j}_* \times \boldsymbol{j}_{*_d} + \boldsymbol{k}_* \times \boldsymbol{k}_{*_d}\right)\ (* = 0, e) \tag{19}$$

where $\boldsymbol{i}_*$, $\boldsymbol{j}_*$ and $\boldsymbol{k}_*$ are unit vectors along the axes of Σ_* with respect to Σ_I, and these vectors can be obtained from the rotational matrix (Luh et al., 1980):

$$\begin{bmatrix}\boldsymbol{i}_* & \boldsymbol{j}_* & \boldsymbol{k}_*\end{bmatrix} = {}^I\boldsymbol{R}_* .$$

Using Equations (13) and (17) actual control input for UVMS is calculated by

$$\boldsymbol{u} = \boldsymbol{M}(\boldsymbol{q})\boldsymbol{\alpha}^{\mathrm{ref}} + \boldsymbol{N}(\boldsymbol{q},\boldsymbol{\zeta})\boldsymbol{\zeta} + \boldsymbol{f} . \tag{20}$$

Here, we represent the matrices and vectors of Equation (13) to the block matrix form:

$$\boldsymbol{M} = \begin{bmatrix}\boldsymbol{M}_{\mathrm{BB}} & \boldsymbol{M}_{\mathrm{BM}} \\ \boldsymbol{M}_{\mathrm{MB}} & \boldsymbol{M}_{\mathrm{MM}}\end{bmatrix},\ \boldsymbol{N} = \begin{bmatrix}\boldsymbol{N}_{\mathrm{BB}} & \boldsymbol{N}_{\mathrm{BM}} \\ \boldsymbol{N}_{\mathrm{MB}} & \boldsymbol{N}_{\mathrm{MM}}\end{bmatrix},\ \boldsymbol{f}_D = \begin{bmatrix}\boldsymbol{f}_{\mathrm{B}} \\ \boldsymbol{f}_{\mathrm{M}}\end{bmatrix},\ \boldsymbol{u} = \begin{bmatrix}\boldsymbol{u}_{\mathrm{B}} \\ \boldsymbol{u}_{\mathrm{M}}\end{bmatrix}.$$

Then we have the following equation with respect to the input of the vehicle:

$$\boldsymbol{M}_{\mathrm{BB}}\dot{\boldsymbol{\nu}}_0 + \boldsymbol{M}_{\mathrm{BM}}\ddot{\boldsymbol{\phi}} + \boldsymbol{N}_{\mathrm{BB}}\boldsymbol{\nu}_0 + \boldsymbol{M}_{\mathrm{BM}}\dot{\boldsymbol{\phi}} + \boldsymbol{f}_{\mathrm{B}} = \boldsymbol{u}_{\mathrm{B}} . \tag{21}$$

And the time derivative of Equation (8) is

$$\dot{\boldsymbol{s}} = \boldsymbol{C}\dot{\boldsymbol{\nu}}_0 + \boldsymbol{D}\ddot{\boldsymbol{\phi}} + \dot{\boldsymbol{C}}\boldsymbol{\nu}_0 + \dot{\boldsymbol{D}}\dot{\boldsymbol{\phi}} . \tag{22}$$

Comparing with Equations (21) and (22), $\boldsymbol{C} = \boldsymbol{M}_{\mathrm{BB}}$, $\boldsymbol{D} = \boldsymbol{M}_{\mathrm{BM}}$, $\dot{\boldsymbol{C}} = \boldsymbol{N}_{\mathrm{BB}}$, $\dot{\boldsymbol{D}} = \boldsymbol{N}_{\mathrm{BM}}$ and $\dot{\boldsymbol{s}} = \boldsymbol{u}_{\mathrm{B}} - \boldsymbol{f}_{\mathrm{B}}$ are obtained. Moreover,

$$\dot{\boldsymbol{A}} = \begin{bmatrix}\boldsymbol{0} & -\left(\tilde{\dot{\boldsymbol{p}}}_e - \tilde{\dot{\boldsymbol{r}}}_0\right) \\ \boldsymbol{0} & \boldsymbol{0}\end{bmatrix},$$

$$\dot{\boldsymbol{B}} = \begin{bmatrix}\boldsymbol{b}_1 & \boldsymbol{b}_2 & \cdots & \boldsymbol{b}_n \\ \boldsymbol{\omega}_1 \times \boldsymbol{k}_1 & \boldsymbol{\omega}_1 \times \boldsymbol{k}_2 & \cdots & \boldsymbol{\omega}_1 \times \boldsymbol{k}_n\end{bmatrix}$$

where $\boldsymbol{b}_i = (\boldsymbol{\omega}_i \times \boldsymbol{k}_i) \times (\boldsymbol{p}_e - \boldsymbol{p}_i) + \tilde{\boldsymbol{k}}_i(\dot{\boldsymbol{p}}_e - \dot{\boldsymbol{p}}_i)$. Therefore, all elements of $\boldsymbol{W}$ and $\dot{\boldsymbol{W}}$ in Equation (16) can be calculated.

3.2 Disturbance compensation of vehicle

From the viewpoint of underwater robot control, parameters and coefficients of hydrodynamic models are generally used as constant values that depend on the shape of robots (Fossen, 1995). The RAC law (17) can reduce the influence of the modelling errors of hydrodynamics by position and velocity feedbacks. Here, to obtain higher control performance, the influence of hydrodynamic modelling error with respect to the vehicle is treated as a disturbance and a disturbance compensation method is introduced.

First, the basic disturbance compensation is described. For $\boldsymbol{M}_{\mathrm{BB}}$ in Equation (21) the nominal model using constant values of added mass, added moment of inertia and drag coefficient is defined as $\overline{\boldsymbol{M}}_{\mathrm{BB}}$. Moreover, the basic disturbance is defined as

$$\boldsymbol{f}_L = \boldsymbol{u}_{\mathrm{B}} - \overline{\boldsymbol{M}}_{\mathrm{BB}}\dot{\boldsymbol{\nu}}_0 , \tag{23}$$

and the estimated value is calculated by

$$\hat{f}_L = F(p)\left(\boldsymbol{u}_{\mathrm{B}} - \overline{\boldsymbol{M}}_{\mathrm{BB}}\dot{\boldsymbol{\nu}}_0\right) \tag{24}$$

where $F(p) = 1/(T_f p + 1)$ is a low pass filter with a time constant T_f and p is the time differentiation operator.

Therefore, for the reference acceleration of vehicle $\dot{\boldsymbol{\nu}}_0^{\mathrm{ref}}$, the control input with disturbance compensation becomes

$$\boldsymbol{u}_{\mathrm{B}} = \overline{\boldsymbol{M}}_{\mathrm{BB}}\dot{\boldsymbol{\nu}}_0^{\mathrm{ref}} + \hat{\boldsymbol{f}}_L, \tag{25}$$

and the configuration of the basic disturbance compensation is shown in Figure 3(a).

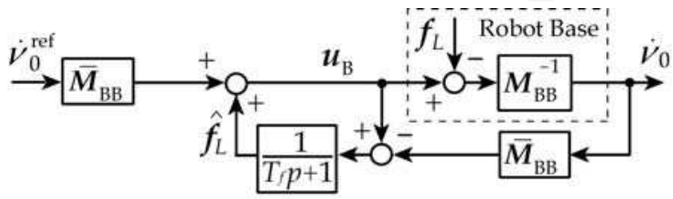

(a) Basic disturbance compensation

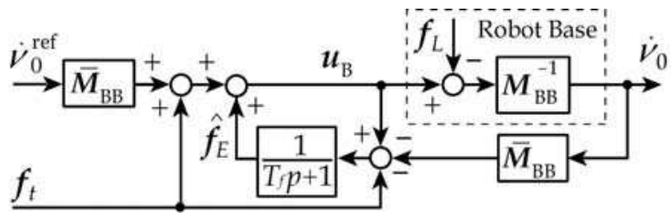

(b) Modified disturbance compensation

Fig. 3. Configuration of disturbance compensation

Next, the basic disturbance compensation is modified. For $\boldsymbol{M}_{\mathrm{BM}}$, $\boldsymbol{N}_{\mathrm{BB}}$, $\boldsymbol{N}_{\mathrm{BM}}$ and $\boldsymbol{f}_{\mathrm{B}}$ in Equation (21) the nominal models using constant values of added mass, added moment of inertia and drag coefficient are defined as $\overline{\boldsymbol{M}}_{\mathrm{BM}}$, $\overline{\boldsymbol{N}}_{\mathrm{BB}}$, $\overline{\boldsymbol{N}}_{\mathrm{BM}}$ and $\bar{\boldsymbol{f}}_{\mathrm{B}}$, respectively. Then the vehicle control input with these nominal models and the reference acceleration $\boldsymbol{\alpha}^{\mathrm{ref}}$ becomes

$$\overline{\boldsymbol{u}}_{\mathrm{B}} = \overline{\boldsymbol{M}}_{\mathrm{BB}}\dot{\boldsymbol{\nu}}_0^{\mathrm{ref}} + \boldsymbol{f}_t \tag{26}$$

where

$$\boldsymbol{f}_t = \overline{\boldsymbol{M}}_{\mathrm{BM}}\ddot{\boldsymbol{\phi}}^{\mathrm{ref}} + \overline{\boldsymbol{N}}_{\mathrm{BB}}\boldsymbol{\nu}_0 + \overline{\boldsymbol{N}}_{\mathrm{BM}}\dot{\boldsymbol{\phi}} + \bar{\boldsymbol{f}}_{\mathrm{B}}. \tag{27}$$

From Equations (23) and (26) the modelling error with respect to the hydrodynamics can be defined as

$$\boldsymbol{f}_E = \boldsymbol{u}_{\mathrm{B}} - \overline{\boldsymbol{M}}_{\mathrm{BB}}\dot{\boldsymbol{\nu}}_0 - \boldsymbol{f}_t, \tag{28}$$

and the estimated value is calculated by

$$\hat{\boldsymbol{f}}_E = F(p)\left(\boldsymbol{u}_{\mathrm{B}} - \overline{\boldsymbol{M}}_{\mathrm{BB}}\dot{\boldsymbol{\nu}}_0 - \boldsymbol{f}_t\right). \tag{29}$$

Therefore, the control input with disturbance compensation becomes

$$\boldsymbol{u}_{\mathrm{B}} = \overline{\boldsymbol{M}}_{\mathrm{BB}}\dot{\boldsymbol{\nu}}_0^{\mathrm{ref}} + \boldsymbol{f}_t + \hat{\boldsymbol{f}}_L \tag{30}$$

and the configuration of the modified disturbance compensation is shown in Figure 3(b).

4. Experiment of continuous-time RAC

In this section, some experiments of the RAC method are done for the vertical type 2-link underwater robot shown in Figure 1.

4.1 Experimental system

Figure 4 shows the configuration of the experimental system. A robot has a 2-DOF manipulator with joints that are actively rotated by velocity and torque control type servo actuators consisting of servo motors and incremental type encoders. The physical parameters of the underwater robot are shown in Table 1. Moreover, four 40[W] thrusters are attached to the vertical and horizontal directions on the robot base to provide propulsion for controlling the position and attitude angle of the base. The forward and reverse propulsion generated by the thruster are calculated by

$$F = \begin{cases} 1.341v^2 - 1.363v - 0.026 & (1.2 \le v \le 4) \\ -0.763v^2 - 0.835v + 0.019 & (-4 \le v \le -1.2) \end{cases} \tag{31}$$

where v is the input voltage to the power amplifier of the thruster. Note that Equation (31) were obtained from the experiments (Yamada & Sagara, 2002).

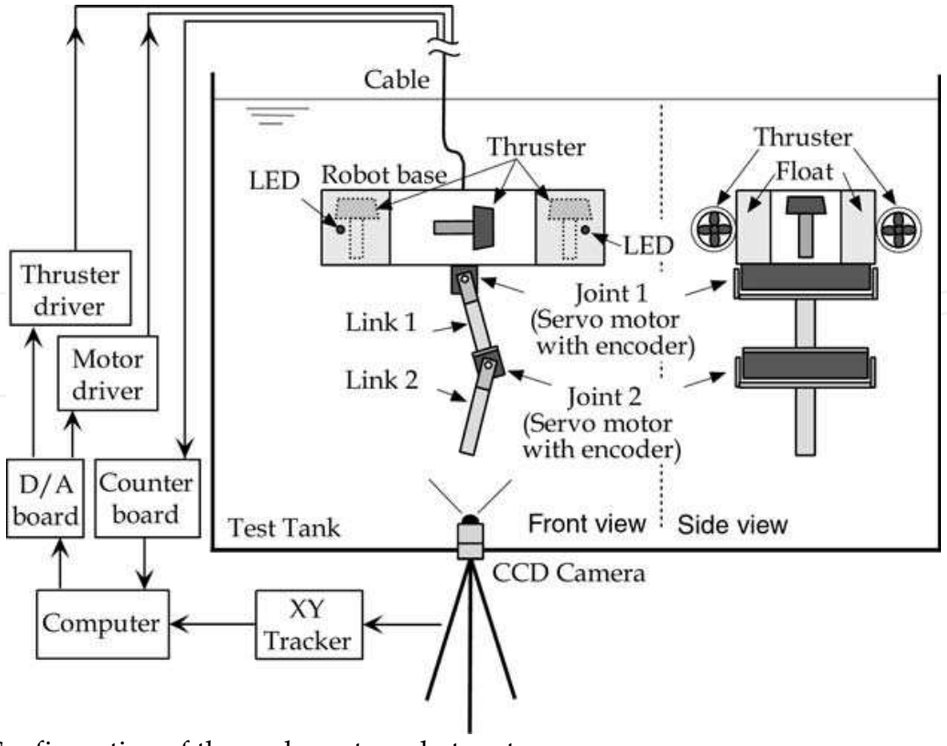

Fig. 4. Configuration of the underwater robot system

The measurement and control system consist of a CCD camera, a video tracker, and a personal computer (PC). Two LEDs are attached to the base, and their motion is monitored by the CCD camera. Video signals of the LED markers are transformed into position data by the video tracker, and put into the PC via a GPIB communication line. Using the position data and the rotational angle of each joint measured by the encoder, the positions and attitude angles of the robot base and manipulator are computed in the PC. The PC is also used as a controller.

	Base	Link 1	Link 2
Mass (kg)	26.04	4.25	1.23
Moment of inertia ($\mathrm{kg}\cdot\mathrm{m}^2$)	1.33	0.19	0.012
Link length (x_i direction) (m)	0.2	0.25	0.25
Link length (z_i direction) (m)	0.81	0.04	0.04
Link width (m)	0.42	0.12	0.12
Added mass (x_i direction) (kg)	72.7	1.31	0.1
Added mass (z_i direction) (kg)	6.28	3.57	2.83
Added moment of inertia ($\mathrm{kg}\cdot\mathrm{m}^2$)	1.05	0.11	0.06
Drag coefficient (x_i direction)	1.2	0	0
Drag coefficient (z_i direction)	1.2	1.2	1.2

Table 1. Physical parameters of underwater robot

4.1 Comparison of control performance of RAC and computed torque methods

In this subsection, to compare the control performances of the RAC method and a computed torque method that is generally used to control of UVMS, simulations and experiments are done. Note that joint torque control type servo actuators are used in the experiments.

Model of vertical type 2-link underwater robot is shown in Figure 5. In this figure F_i (i = 1, 2, 3) is the thrust of thruster and R is a distance from the origin of Σ_0 to the thruster. For the model shown in Figure 5 kinematic, momentum and dynamic Equations (3), (8) and (13) are reduced to

$$\dot{\boldsymbol{p}}_{e_V} = \boldsymbol{A}_V \dot{\boldsymbol{x}}_{0_V} + \boldsymbol{B}_V \dot{\boldsymbol{\phi}}_V , \tag{32}$$

$$\boldsymbol{s}_V = \boldsymbol{C}_V \dot{\boldsymbol{x}}_{0_V} + \boldsymbol{D}_V \dot{\boldsymbol{\phi}}_V , \tag{33}$$

$$\boldsymbol{M}_V(\boldsymbol{q}_V)\ddot{\boldsymbol{q}}_V + \boldsymbol{N}_V(\boldsymbol{q}_V, \dot{\boldsymbol{q}}_V)\dot{\boldsymbol{q}}_V + \boldsymbol{f}_V = \boldsymbol{u}_V \tag{34}$$

where

$$\boldsymbol{p}_{e_V} = \begin{bmatrix} p_{e_x} \\ p_{e_z} \end{bmatrix},\ \boldsymbol{x}_{0_V} = \begin{bmatrix} r_{0_x} \\ r_{0_z} \\ \phi_0 \end{bmatrix}, \boldsymbol{\phi}_V = \begin{bmatrix} \phi_1 \\ \phi_2 \end{bmatrix},\ \boldsymbol{q}_V = \begin{bmatrix} \boldsymbol{x}_{0_V} \\ \boldsymbol{\phi}_V \end{bmatrix},\ \boldsymbol{u}_V = \begin{bmatrix} \boldsymbol{u}_{\mathrm{B}_V} \\ \boldsymbol{u}_{\mathrm{M}_V} \end{bmatrix},\ \boldsymbol{u}_{\mathrm{B}_V} = \begin{bmatrix} f_{0_x} \\ f_{0_z} \\ \tau_0 \end{bmatrix},\ \boldsymbol{u}_{\mathrm{M}_V} = \begin{bmatrix} \tau_1 \\ \tau_2 \end{bmatrix},$$

and $\boldsymbol{A}_V$, $\boldsymbol{B}_V$, $\boldsymbol{D}_V$, $\boldsymbol{C}_V$ and $\boldsymbol{s}_V$ are appropriate matrices and vector.

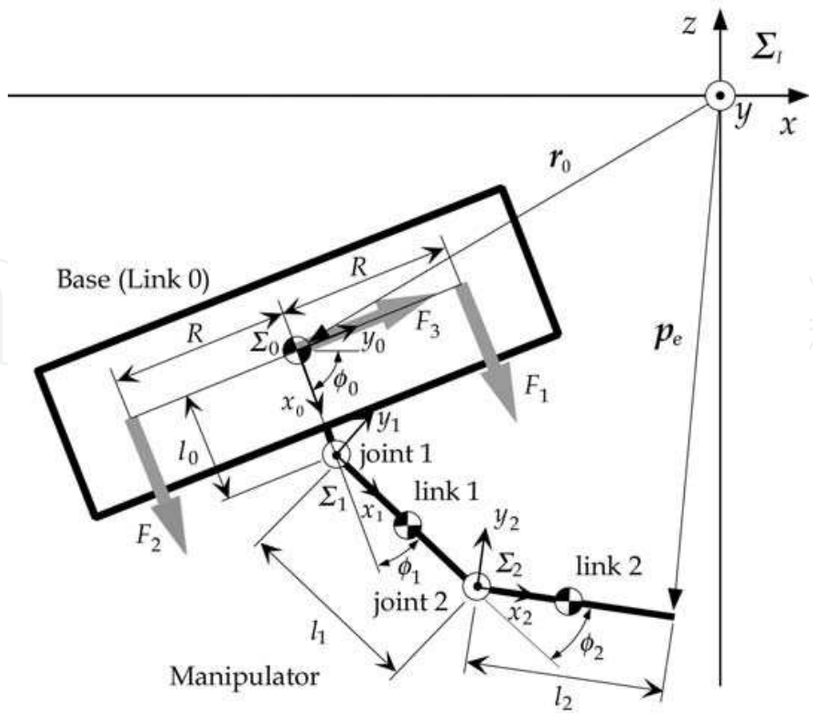

Fig. 5. Model of vertical type 2-link underwater robot

Similarly, the RAC law (17) is reduced to

$$\boldsymbol{\alpha}_V^{\mathrm{ref}}(t) = \boldsymbol{W}_V^{\#}(t)\{\boldsymbol{\beta}_V^{\mathrm{ref}}(t) + \boldsymbol{\gamma}_V(t) - \dot{\boldsymbol{W}}_V(t)\dot{\boldsymbol{q}}_V(t)\} \tag{35}$$

where

$$\boldsymbol{\beta}_V^{\mathrm{ref}} = \begin{bmatrix} \ddot{\boldsymbol{x}}_{0_V}^{\mathrm{des}} \\ \ddot{\boldsymbol{p}}_{e_V}^{\mathrm{des}} \end{bmatrix} + \boldsymbol{K}_{V_V}\begin{bmatrix} \dot{\boldsymbol{x}}_{0_V}^{\mathrm{des}} - \dot{\boldsymbol{x}}_{0_V} \\ \dot{\boldsymbol{p}}_{e_V}^{\mathrm{des}} - \dot{\boldsymbol{p}}_{e_V} \end{bmatrix} + \boldsymbol{K}_{P_V}\begin{bmatrix} \boldsymbol{x}_{0_V}^{\mathrm{des}} - \boldsymbol{x}_{0_V} \\ \boldsymbol{p}_{e_V}^{\mathrm{des}} - \boldsymbol{p}_{e_V} \end{bmatrix}, \tag{36}$$

$$\boldsymbol{W}_V = \begin{bmatrix} \boldsymbol{C}_V + \boldsymbol{E}_3 & \boldsymbol{D}_V \\ \boldsymbol{A}_V & \boldsymbol{B}_V \end{bmatrix}, \quad \boldsymbol{\gamma}_V = \begin{bmatrix} \dot{\boldsymbol{s}}_V \\ \boldsymbol{0} \end{bmatrix},$$

and $\boldsymbol{\alpha}_V^{\mathrm{ref}}$ is the reference of $\boldsymbol{\alpha}_V (= \ddot{\boldsymbol{q}}_V)$, $\boldsymbol{K}_{V_V}$ and $\boldsymbol{K}_{P_V}$ are positive diagonal matrices.

On the other hand, a computed torque method is briefly described as follows. From Equation (32) the task-space velocity $\boldsymbol{\nu}_V = [\dot{\boldsymbol{x}}_{0_V}^T \quad \dot{\boldsymbol{p}}_{e_V}^T]^T$ and joint–space velocity $\dot{\boldsymbol{q}}_V$ are related as

$$\boldsymbol{\nu}_V(t) = \boldsymbol{J}(t)\dot{\boldsymbol{q}}_V(t) \tag{37}$$

where

$$\boldsymbol{J} = \begin{bmatrix} \boldsymbol{E}_3 & \boldsymbol{0} \\ \boldsymbol{A}_V & \boldsymbol{B}_V \end{bmatrix}.$$

From Equation (37) the following equation can be obtained:

$$\ddot{\boldsymbol{q}}_V(t) = \boldsymbol{J}^{\#}(t)\{\dot{\boldsymbol{\nu}}_V(t) - \dot{\boldsymbol{J}}(t)\dot{\boldsymbol{q}}_V(t)\}\,. \tag{38}$$

For Equation (38) reference joint-space acceleration is defined as

$$\ddot{\boldsymbol{q}}_V^{\mathrm{ref}}(t) = \boldsymbol{J}^{\#}(t)\{\dot{\boldsymbol{\nu}}_V^{\mathrm{ref}}(t) - \dot{\boldsymbol{J}}(t)\dot{\boldsymbol{J}}^{\#}(t)\boldsymbol{\nu}_V^{\mathrm{ref}}(t)\}\,. \tag{39}$$

Based on Equations (34) and (39) actual control input is calculated by using the following equation:

$$\boldsymbol{M}_V\ddot{\boldsymbol{q}}_V^{\mathrm{des}} + \boldsymbol{N}_V\dot{\boldsymbol{q}}_V + \boldsymbol{f}_V = \boldsymbol{u}_V \tag{40}$$

where

$$\boldsymbol{q}_V^{\mathrm{des}} = \boldsymbol{q}_V^{\mathrm{ref}} + \overline{\boldsymbol{K}}_{V_V}(\dot{\boldsymbol{q}}_V^{\mathrm{ref}} - \dot{\boldsymbol{q}}_V) + \overline{\boldsymbol{K}}_{P_V}(\boldsymbol{q}_V^{\mathrm{ref}} - \boldsymbol{q}_V)\,, \tag{41}$$

and $\overline{\boldsymbol{K}}_{V_V}$ and $\overline{\boldsymbol{K}}_{P_V}$ are positive diagonal matrices.

Both simulations and experiments are carried out under the following condition. The desired end-tip position is set up along a straight path from the initial position to the target. On the other hand, the desired position and attitude of the base are set up the initial values. The feedback gains are $\boldsymbol{K}_{V_V} = \overline{\boldsymbol{K}}_{V_V} = \mathrm{diag}\{10 \quad 10 \quad 10 \quad 10 \quad 10\}$ and $\boldsymbol{K}_{P_V} = \overline{\boldsymbol{K}}_{P_V} = \mathrm{diag}\{100 \quad 100 \quad 100 \quad 50 \quad 50\}$. The initial relative joint angles are $\phi_0 = -\pi/2$ [rad], $\phi_1 = \pi/3$ [rad] and $\phi_2 = -5\pi/18$ [rad].

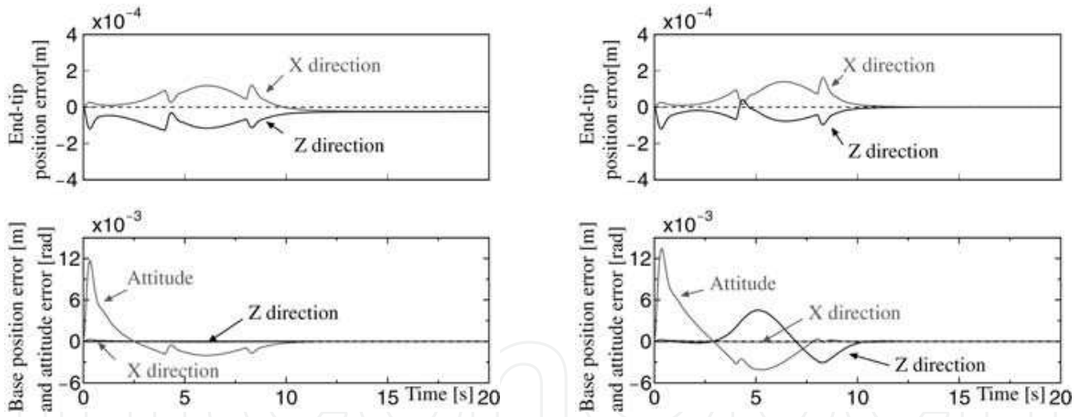

(a) Computed torque method (b) RAC method

Fig. 6. Simulation results of computed torque method and RAC method

First, simulation results of the computed torque method and the RAC method are shown in Figure 6(a) and (b). From Figure 6 we can see that both control methods have similar performance.

Next, we show the experimental results. As a computer is used for a controller in experiments, the sampling period for the controller is set up to $T = 1/60$ [s]. Figure 7 shows the both experimental results. From this figure, we can see that the performance of the computed torque method becomes worse. Since the computed torque method only uses joint-space errors, the control performance of the end-tip of the manipulator depends on the

robot base (vehicle) control performance. Therefore, if the acceleration and velocity relations between the end-tip and joints are inaccurate or the control performance of the vehicle is not better, good control performance of the end-tip cannot be obtained. On the other hand, from Figure 7 it can be seen that the RAC method has good control performance.

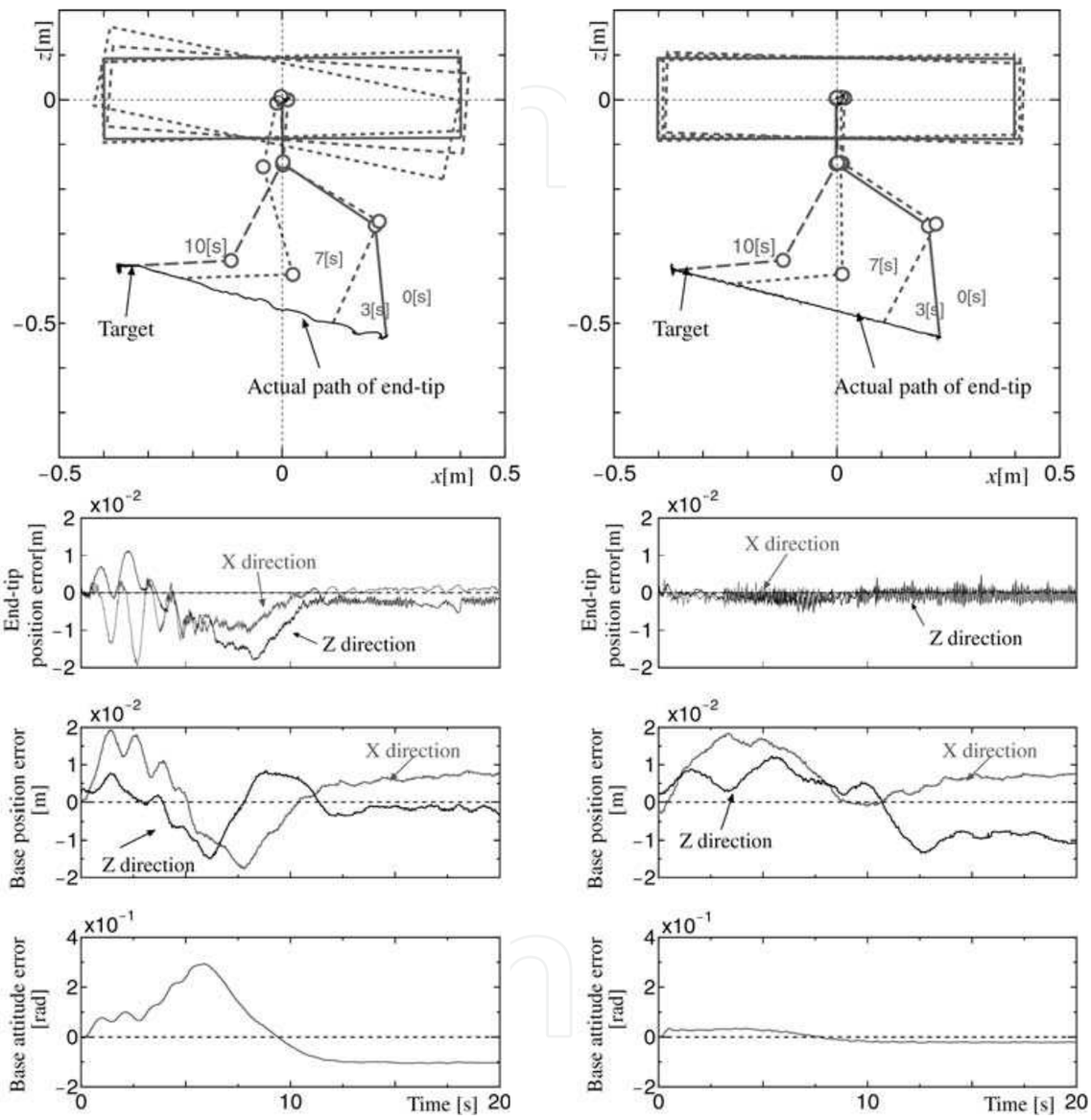

(a) Computed torque method (b) RAC method

Fig. 7. Experimental results of computed torque method and RAC method

4.2 RAC method with disturbance compensation of vehicle

Experiments are carried out under the following condition. The desired end-tip position is set up along a straight path from the initial position to the target. On the other hand, the desired position and attitude of the base are set up the initial values. The feedback gains are

$\boldsymbol{K}_{V_V} = \mathrm{diag}\{10 \quad 10 \quad 10 \quad 20 \quad 20\}$ and $\boldsymbol{K}_{P_V} = \mathrm{diag}\{100 \quad 100 \quad 100 \quad 100 \quad 100\}$. The time constant of filter is $T_f = 1$ [s]. In this case joint velocity control type actuators are used.

Figure 8 shows the motion of the robot and estimated disturbance of the RAC with disturbance compensation, and Figure 9 shows the time histories of experimental results with and without disturbance compensation. Form Figures 8 and 9, it can be seen that the end-tip of manipulator follows the desired trajectory. Moreover, since the robot base position and attitude errors become small values using the disturbance compensation, the end-tip position error is also reduced.

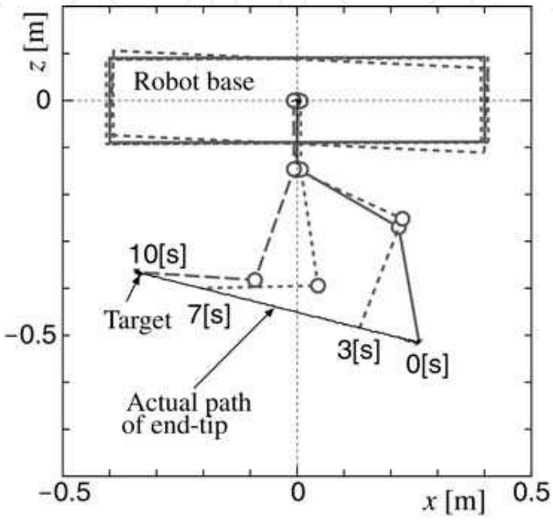

(a) Motion

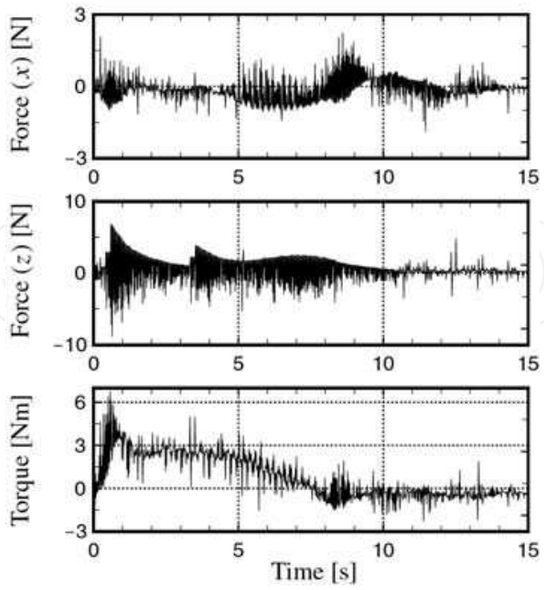

(b) Estimated disturbance

Fig. 8. Experimental result of RAC method with disturbance compensation

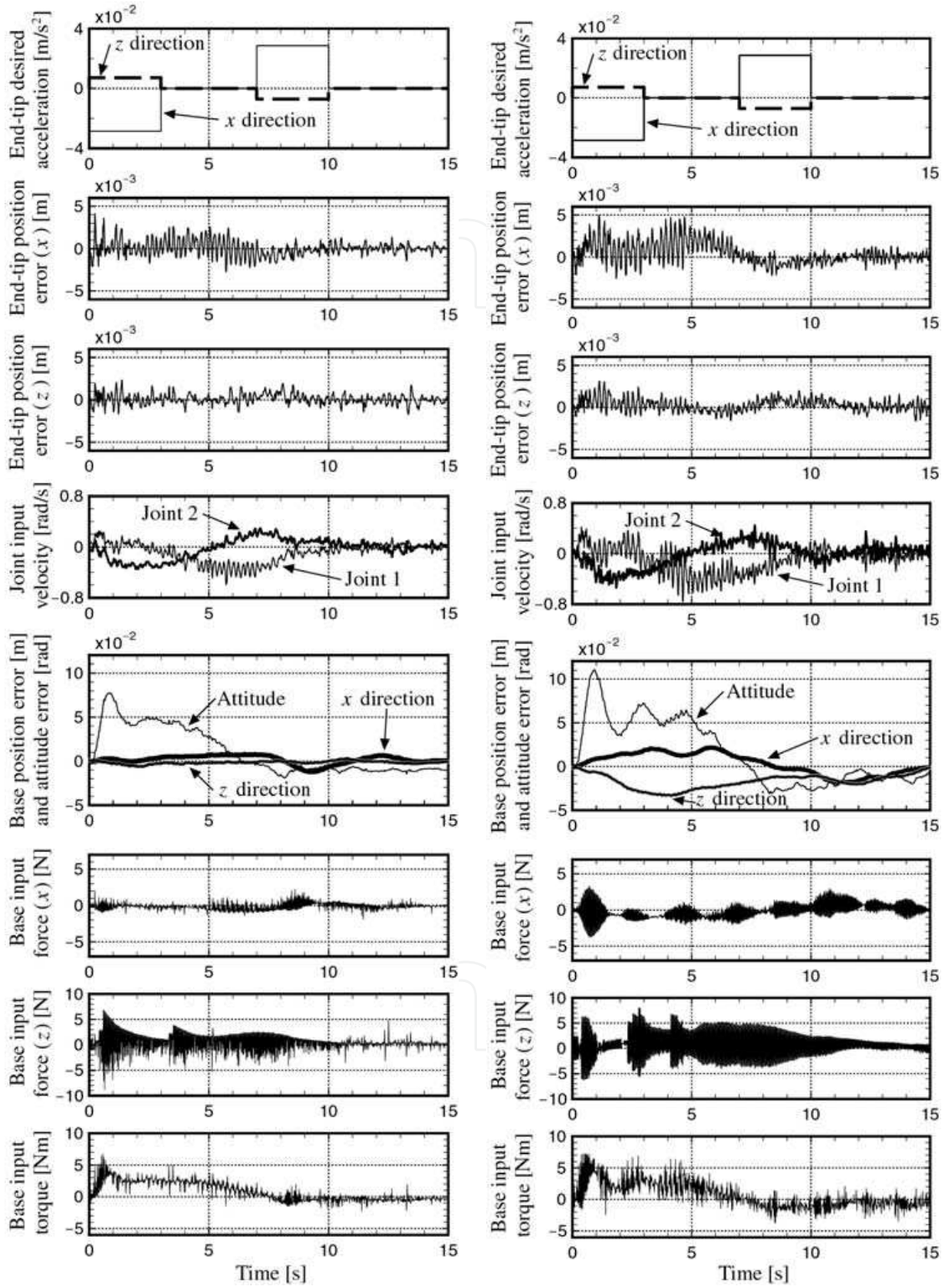

(a) RAC with disturbance compensation (b) RAC without disturbance compensation

Fig. 9. Experimental results of RAC method with and without disturbance compensation

5. Discrete-time RAC

In practical systems digital computers are utilized for controllers, but there is no discrete-time control method for UVMS except our proposed methods (Sagara, 2003; Sagara et al., 2004; Sagara et al., 2006; Yatoh & Sagara, 2008). In this section, we address discrete time RAC methods including the ways of disturbance compensation of the vehicle and avoidance of singular configuration of the manipulator.

5.1 Discrete-time RAC law

Discretizing Equation (16) by a sampling period T, and applying $\boldsymbol{\beta}(k)$ and $\dot{\boldsymbol{W}}(k)$ to the backward Euler approximation, the following equation can be obtained:

$$\boldsymbol{W}(k)\boldsymbol{\alpha}(k-1)=\frac{1}{T}\{\boldsymbol{\nu}(k)-\boldsymbol{\nu}(k-1)+T\boldsymbol{\gamma}(k)-[\boldsymbol{W}(k)-\boldsymbol{W}(k-1)]\boldsymbol{\zeta}(t)\} \tag{42}$$

where $\boldsymbol{\nu}=[\boldsymbol{\nu}_0^T \quad \boldsymbol{\nu}_e^T]^T$. Note that a computational time delay is introduced into Equation (42), and the discrete time kT is abbreviated to k.
For Equation (42), the desired acceleration is defined as

$$\boldsymbol{\alpha}_d(k)=\frac{1}{T}\boldsymbol{W}^{\#}(k)\{\boldsymbol{\nu}_d(k+1)-\boldsymbol{\nu}_d(k)+\boldsymbol{\Lambda}\boldsymbol{e}_\nu(k)+T\boldsymbol{\gamma}(k)\} \tag{43}$$

where

$$\boldsymbol{e}_\nu(k)=\boldsymbol{\nu}_d(k)-\boldsymbol{\nu}(k) \tag{44}$$

and $\boldsymbol{\nu}_d(k)$ is the desired value of $\boldsymbol{\nu}(k)$, $\boldsymbol{\Lambda}=\mathrm{diag}\{\lambda_i\}$ ($i=1,\cdots,12$) is the velocity feedback gain matrix.
From Equations (42) and (43) we have

$$T\boldsymbol{W}(k)\boldsymbol{e}_\alpha(k-1)=\boldsymbol{e}_\nu(k)-\boldsymbol{e}_\nu(k-1)+\boldsymbol{\Lambda}\boldsymbol{e}_\nu(k)-T\{\boldsymbol{\gamma}(k)-\boldsymbol{\gamma}(k-1)\}+\{\boldsymbol{W}(k)-\boldsymbol{W}(k-1)\}\boldsymbol{\zeta}(t) \tag{45}$$

where

$$\boldsymbol{e}_\alpha(k)=\boldsymbol{\alpha}_d(k)-\boldsymbol{\alpha}(k).$$

Assuming $\boldsymbol{W}(k)\approx\boldsymbol{W}(k-1)$ and $\boldsymbol{\gamma}(k)\approx\boldsymbol{\gamma}(k-1)$ for one sampling period, Equation (45) can be rewritten as

$$T\boldsymbol{W}(k)\boldsymbol{e}_\alpha(k-1)=\{(q-1)\boldsymbol{E}_{12}+\boldsymbol{\Lambda}\}\boldsymbol{e}_\nu(k) \tag{46}$$

where q is the forward shift operator. Since all elements of $\boldsymbol{W}(k)$ are bounded, if λ_i is selected to satisfy $0<\lambda_i<1$ and the convergence of $\boldsymbol{e}_\alpha(k)$ tends to zero as k tends to infinity, the convergence of $\boldsymbol{e}_\nu(k)$ to zero as k tends to infinity can be ensured from Equation (46).
Moreover, the desired velocity of $\boldsymbol{\nu}(k)$ is defined as

$$\boldsymbol{\nu}_d(k)=\frac{1}{T}\boldsymbol{S}_{0e}(k)\{\boldsymbol{x}_d(k)-\boldsymbol{x}_d(k-1)+\boldsymbol{\Gamma}\boldsymbol{e}_x(k-1)\} \tag{47}$$

where

$$S_{0e}=\begin{bmatrix} E_3 & & & \mathbf{0} \\ & S_{\psi_0} & & \\ & & E_3 & \\ \mathbf{0} & & & S_{\psi_e} \end{bmatrix},\quad e_x(k)=x_d(k)-x(k),\quad x=\begin{bmatrix} r_0 \\ \psi_0 \\ p_e \\ \psi_e \end{bmatrix},$$

and $x_d(k)$ is the desired value of $x(k)$ ($=[x_0^T \quad x_e^T]^T$), $\Gamma=\mathrm{diag}\{\gamma_i\}$ ($i=1,\cdots,12$) is the position feedback gain matrix.
From Equations (44) - (47) the following equation can be obtained:

$$Te_v(k)=S_{0e}\{E_{12}-(E_{12}-\Gamma)q^{-1}\}e_x(k) \tag{48}$$

where $\nu(k)$ is applied to the backward Euler approximation. From Equation (48), if γ_i is selected to satisfy $0<\gamma_i<1$ and the convergence of $e_v(k)$ tends to zero as k tends to infinity, the convergence of $e_x(k)$ to zero as k tends to infinity can be ensured.
The configuration of the control system described in this subsection is shown in Figure 10.

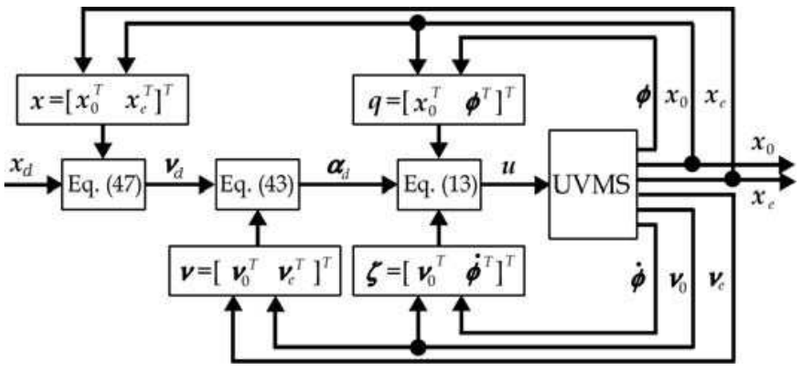

Fig. 10. Control system of discrete-time RAC

5.2 Disturbance compensation of vehicle

Discretizing the low pass filter, $F(p)=1/(T_f p+1)$, shown in Figure 3(b) (Godler et al., 2002), a digital version of disturbance compensation can be obtained. Figure 11 shows the digital version where $h=e^{-T_f/T}$.

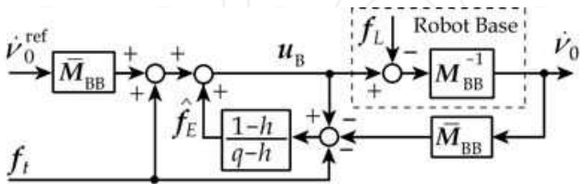

Fig. 11. Digital type disturbance compensation

5.3 Avoidance of a singular configuration

In much work on UVMS it is considered that the vehicle is keeping its initial state during the manipulation. In order to avoid the singular configuration of the manipulator in such case, the desired value of the vehicle is modified by using the determinant of the manipulator's Jacobian matrix $J(k)=\det \boldsymbol{J}(k)$ (Sagara et al., 2006).
The desired linear acceleration of the vehicle is defined as

$$\ddot{\boldsymbol{r}}_{0_d}(k) = \begin{cases} \dot{\boldsymbol{p}}_{e_d}(k) & (k_a \le k \le k_a + n_a) \\ \boldsymbol{0} & (\text{otherwise}) \\ -\dot{\boldsymbol{p}}_{e_d}(k) & (k_s \le k \le k_s + n_a) \end{cases} \tag{49}$$

where $\dot{\boldsymbol{p}}_{e_d}$ is the desired linear velocity of the end-tip of the manipulator, and $k_a T$ and $k_s T$ are the time when $|J(k)|$ becomes less or greater than a threshold J_s , respectively, and $n_a T$ is the acceleration time.

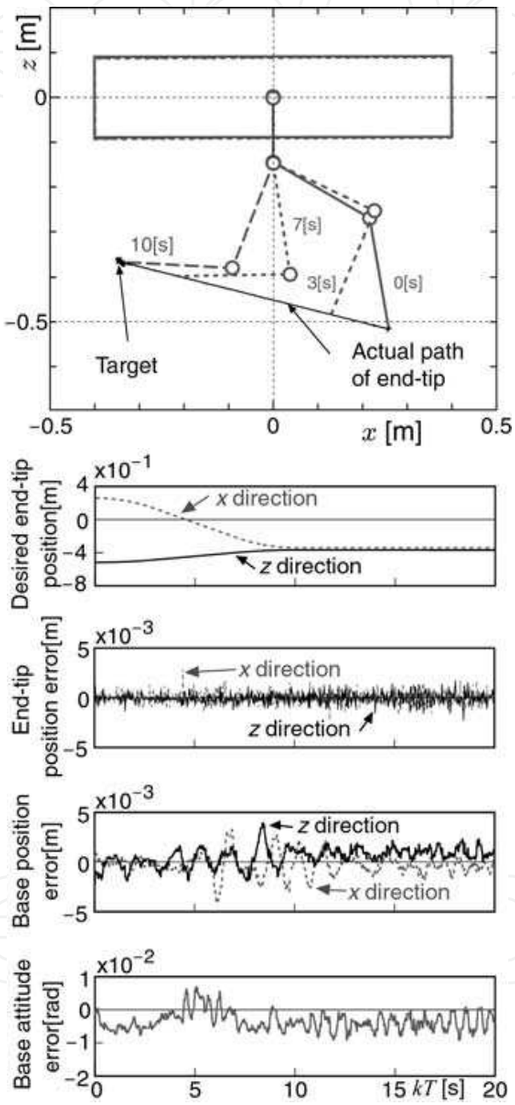

Fig. 12. Experimental result of discrete-time RAC

5.4 Experiment of discrete-time RAC

In this subsection, some experiments of the discrete-time RAC method described above are done for the underwater robot shown in Figures 1 and 4.

All experiments are carried out under the following condition. The desired end-tip position is set up along a straight path from the initial position to the target. On the other hand, the

desired position and attitude of the base are set up the initial values. The sampling period is $T = 1/60$ [s] based on the processing time of video tracker.

First, a basic discrete-time RAC experiment is done. In this case, the feedback gains are $\boldsymbol{\Lambda} = \mathrm{diag}\{0.6 \quad 0.6 \quad 0.25 \quad 0.25 \quad 0.25\}$ and $\boldsymbol{\Gamma} = \mathrm{diag}\{0.3 \quad 0.3 \quad 0.25 \quad 0.25 \quad 0.25\}$. Figure 12 shows the experimental result. From this figure, it can be seen that the discrete-time RAC method has good control performance and the performance is similar to that of the continuous-time version shown in Figure 7(b).

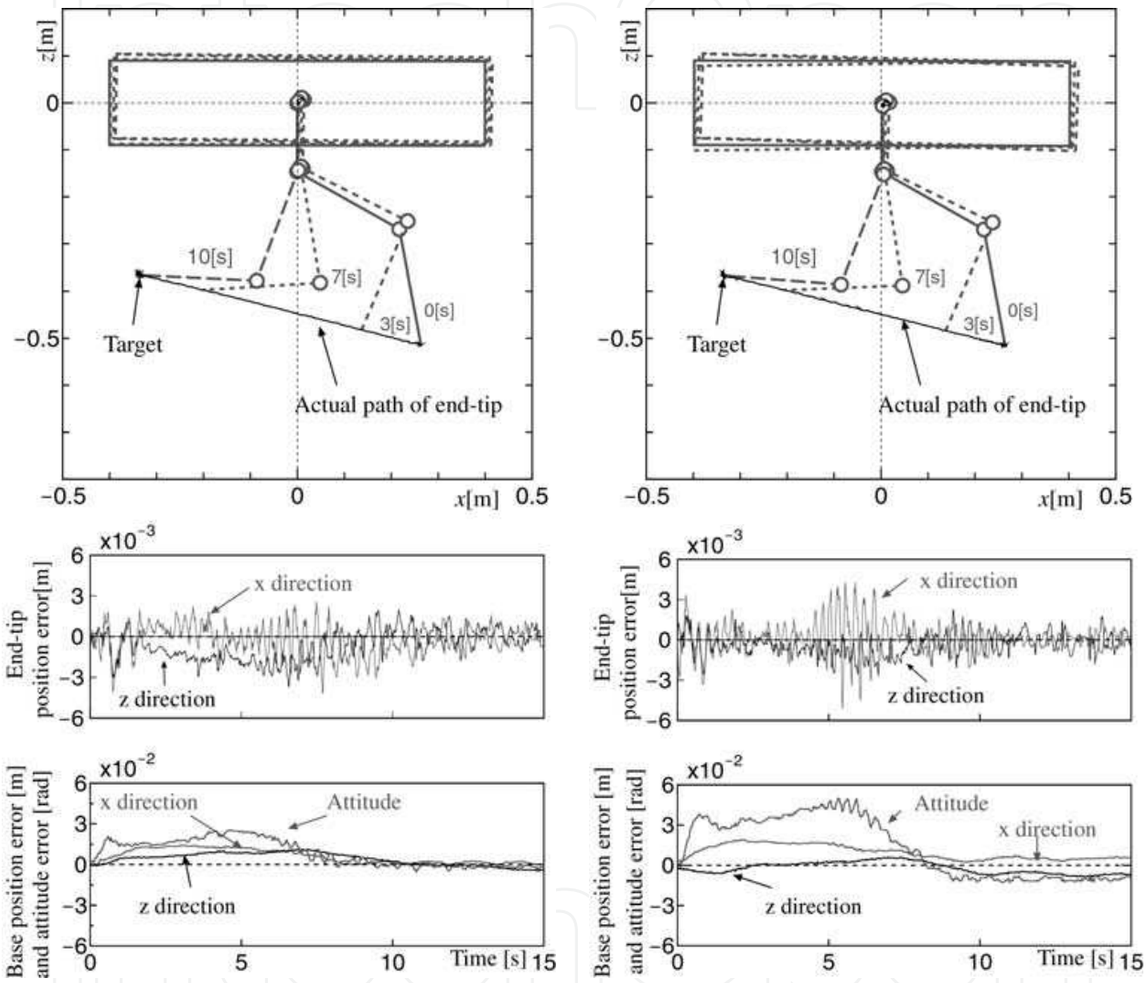

(a) RAC with disturbance compensation (b) RAC without disturbance compensation

Fig. 13. Experimental results of discrete-time RAC with and without disturbance compensation

Next, experiments of discrete-time RAC with and without disturbance compensation of the base are done. To validate the performance of disturbance compensation, the feedback gains of the RAC are $\boldsymbol{\Lambda} = \boldsymbol{\Gamma} = \mathrm{diag}\{0.3 \quad 0.3 \quad 0.2 \quad 0.2 \quad 0.2\}$. Using these values of the gains the basic control performance of the RAC becomes worse. The time constant of the filter for the disturbance compensation is $T_f = 0.1$ [s]. The experimental results of the RAC with and without disturbance compensation are shown in Figure 13(a) and (b), respectively. And Figure 14 shows the time history of the estimated disturbance. From Figures 13 and 14, it

can be seen that the position and attitude errors of the base are reduced by using the disturbance compensation.

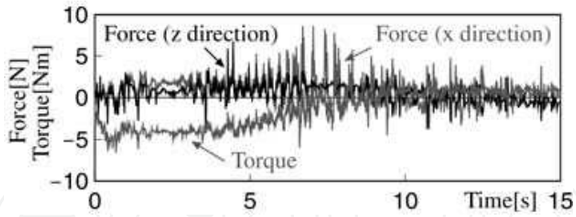

Fig. 14. Estimated disturbance (digital version)

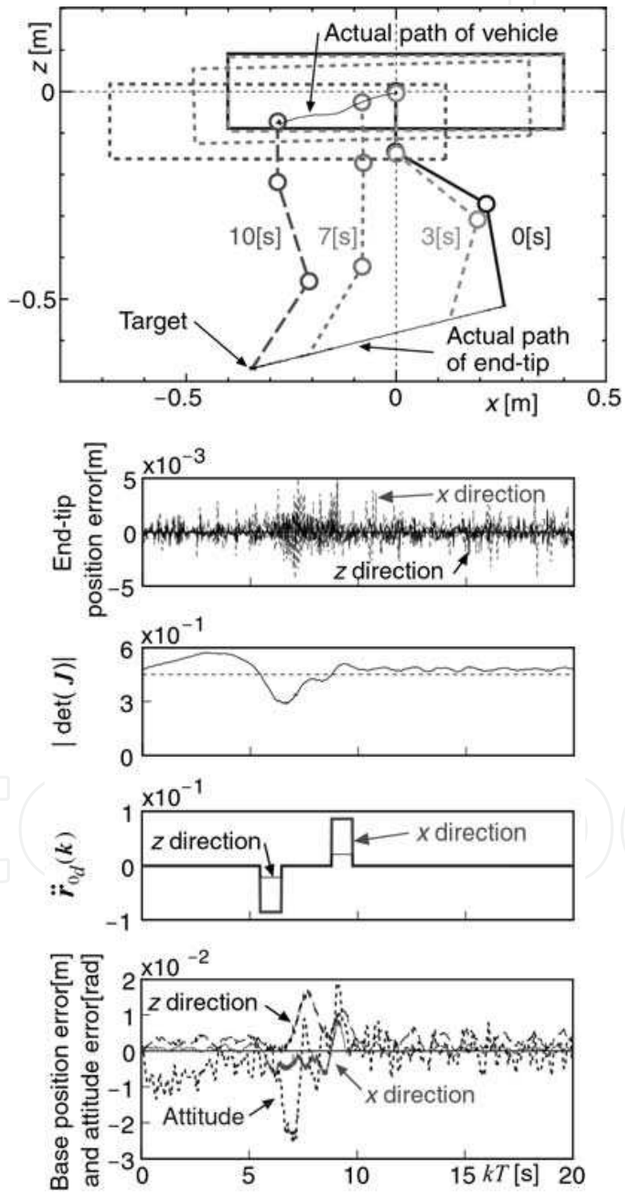

Fig. 15. Experimental result of discrete-time RAC considering singular configuration

Finally, an experiment of avoidance of singular configuration is done. In this case, the basic desired position and attitude of the base (vehicle) is set as the initial values, and the threshold of the determinant of the Jacobian matrix is $J_s = 0.45$. And the feedback gains are $\boldsymbol{\Lambda} = \boldsymbol{\Gamma} = \mathrm{diag}\{0.6 \quad 0.6 \quad 0.25 \quad 0.25 \quad 0.25\}$. The experimental result is shown in Figure 15. From Figure 15, we can see that the end-tip of the manipulator and base follow the desired trajectories avoiding the singular configuration of the manipulator and the tracking errors are very small.

6. Conclusion

In this chapter, our proposed continuous-time and discrete-time RAC methods was described and the both experimental results using a 2-link underwater robot were shown. For the continuous-time RAC method, experimental results showed that the RAC method has good control performance in comparison with a computed torque method and the RAC method with disturbance compensation can reduce the influence of the hydrodynamic modelling error. In practical systems digital computers are utilized for controllers. Then, we addressed discrete-time RAC methods including the ways of disturbance compensation and avoidance of singular configuration. Experimental results show that the control performance of the discrete-time RAC method is similar to the continuous version. Our future work is to carry out experiments in 3-dimensional space to evaluate the validity of the RAC methods.

7. References

Antonelli, G. & Chiaverini, S. (1998). Task-Priority Redundancy Resolution for Underwater Vehicle-Manipulator Systems, *Proceedings of the 1998 IEEE Iinternational Conference on Robotics and Automation*, pp. 768-773, 0-7803-4758-7, Leuven, May 1998

Antonelli, G.; Caccavale, F.; Chiaverini. S. & Villani, L. (2000). Tracking Control for Underwater Vehicle-Manipulator Systems with Velocity Estimation, *IEEE Journal of Oceanic Engineering*, Vol. 25, No. 3, pp. 399-413, 0364-9059

Antonelli, G. (2003). *Underwater Robots: Motion and Force Control of Vehicle-Manipulator Systems*, Springer-Verlag, 3-540-00054-2, Berlin

Fossen, T.I. (1994). *Guidance and Control of Ocean Vehicles*, John Wiley & Sons, 0-471-94113-1, NY

Godler, I.; Honda, H. & Ohnishi, K. (2002). Design Guidance for Disturbance Observer's Filter in Discrete Time, *Proceedings of 7th International Workshop on Advanced Motion Control*, pp. 390-395, 0-7803-7479-7, Maribor, Slovenia, Jul. 2002

Levesque, B. & Richard, M.J. (1994). Dynamic Analysis of a Manipulator in a Fluid Environment, *International Journal of Robotics Research*, Vol. 13, No. 3, pp. 221-231, 0278-3649

Luh, J.Y.S; Walker, M.W. & Paul, R.P.C. (1980). Resolved-Acceleration Control of Mechanical Manipulators, *IEEE Transactions on Automatic Control*, Vol. 25, No. 3, pp. 468-474, 0018-9286

Maheshi, H.; Yuh, J. & Lakshmi, R. (1991). A Coordinated Control of an Underwater Vehicle and Robotic Manipulator, J*ournal of Robotic Systems*, Vol. 8, No. 3, pp. 339-370, 07412223

McLain, T.W.; Rock, S.M. & Lee, M.J. (1996). Experiments in the Coordinated Control of an Underwater Arm/Vehicle System, In: *Underwater Robots*, Yuh, J.; Ura, T. & Bekey, G. A., (Ed), pp.137-158, Kluwer Academic Publishers, 0-7923-9754-1, MA

McLain, T.W. & Rock, S.M. (1998). Development and Experimental Validation of an Underwater Manipulator Hydrodynamic Model, *International Journal of Robotics Research*, Vol. 17, No. 7, pp. 748-759, 0278-3649

McMillan, S.; David, D.E. & McGhee, R.B. (1995). Efficient Dynamic Simulation of an Underwater Vehicle with a Robotic Manipulator, *IEEE Transactions on Systems, Man and Cybernetics*, Vol. 25, No, 8, pp. 1194-1206, 0018-9472

Sagara, S. (2003). Digital Control of an Underwater Robot with Vertical Planar 2-Link Manipulator, *Proceedings of the 8th International Symposium on Artificial Life and Robotics*, pp. 524-527, 4-9900462-3-4, Beppu, Jan. 2003

Sagara, S.; Shibuya. K. & Tamura, M. (2004). Experiment of Digital RAC for an Underwater Robot with Vertical Planar 2-Link Manipulator, *Proceedings of the 9th International Symposium on Artificial Life and Robotics*, pp. 337-340, 4-9900462-4-2, Beppu, Jan. 2004

Sagara, S.; Tamura, M.; Yatoh, T. & Shibuya, K. (2006). Digital RAC for Underwater Vehicle-Manipulator Systems Considering Singular Configuration, *Artificial Life and Robotics,* Vol. 10, No. 2, pp. 106-111, 1433-5298, Springer

Sarkar, N. & Podder, T.K. (2001). Coordinated Motion Planning and Control of Autonomous Underwater Vehicle-Manipulator Systems:Subject to Drag Optimization, *IEEE Journal of Oceanic Engineering*, Vol. 26, No. 2, pp. 228-239, 0364-9059

Tarn, T. J; Shoults, G.A. & Yang, S.P. (1996). A Dynamic Model of an Underwater Vehicle with a Robotic Manipulator Using Kane's Method, In: *Underwater Robots*, Yuh, J.; Ura, T. & Bekey, G. A., (Ed), pp.137-158, Kluwer Academic Publishers, 0-7923-9754-1, MA

Yamada, S. & Sagara, S. (2002). Resolved Acceleration Control of an Underwater Robot with Vertical Planar 2-Link Manipulator, *Proceedings of the 7th International Symposium on Artificial Life and Robotics*, pp. 230-233, 4-9900462-2-6, Beppu, Jan. 2002

Yatoh, T. & Sagara, S. (2007). Resolved Acceleration Control of Underwater Vehicle-Manipulator Systems Using Momentum Equation, *Proceedings of OCEANS 2007 MTS/IEEE Vancouver*, paper number 070427-004, 0-933957-35-1, Vancouver, Oct. 2007

Yatoh, T. & Sagara, S. (2008). Digital Type Disturbance Compensation Control of Underwater Vehicle-Manipulator Systems, *Proceedings of OCEANS'08 MTS/IEEE Kobe-Techno-Ocean'08*, paper number 071109-002, 978-1-4244-2126-8, Kobe, Apr. 2008

Yuh, J. (Ed). (1995). *Underwater Robotic Vehicles: Design and Control*, TSI Press, 0-9627451-6-2, NW

Underwater Vehicles

Edited by Alexander V. Inzartsev

ISBN 978-953-7619-49-7

Hard cover, 582 pages

Publisher InTech

Published online 01, January, 2009

Published in print edition January, 2009

For the latest twenty to thirty years, a significant number of AUVs has been created for the solving of wide spectrum of scientific and applied tasks of ocean development and research. For the short time period the AUVs have shown the efficiency at performance of complex search and inspection works and opened a number of new important applications. Initially the information about AUVs had mainly review-advertising character but now more attention is paid to practical achievements, problems and systems technologies. AUVs are losing their prototype status and have become a fully operational, reliable and effective tool and modern multi-purpose AUVs represent the new class of underwater robotic objects with inherent tasks and practical applications, particular features of technology, systems structure and functional properties.

InTech Europe

University Campus STeP Ri
Slavka Krautzeka 83/A
51000 Rijeka, Croatia
Phone: +385 (51) 770 447
Fax: +385 (51) 686 166
www.intechopen.com

InTech China

Unit 405, Office Block, Hotel Equatorial Shanghai
No.65, Yan An Road (West), Shanghai, 200040, China
中国上海市延安西路65号上海国际贵都大饭店办公楼405单元
Phone: +86-21-62489820
Fax: +86-21-62489821

IntechOpen